Solvation effect of TCNQ and F4-TCNQ Solution on Electrical Properties of Atomically thin MoS_2 Channel FET Equipped with Microfluid Tank

Md Nasiruddin[1], Zhipeng Wang[1], Hiroki Waizumi[1], Tsuyoshi Takaoka[2], Yasuyuki Sainoo[2], Atsushi Ando[3], Ryuichi Arafune[4], Akihide Hibara[2], & Tadahiro Komeda[2]*

1 Department of Chemistry, Graduate School of Science, Tohoku University, Aramaki-Aza-Aoba, Aoba-Ku, Sendai 9808578, Japan

2 Institute of Multidisciplinary Research for Advanced Materials (IMRAM, Tagen), Tohoku University, 2-1-1, Katahira, Aoba-Ku, Sendai 9800877, Japan

3 National Institute of Advanced Industrial Science and Technology, 1-1-1 Umezono, Tsukuba, Ibaraki 305-8568, Japan

4 International Center for Materials Nanoarchitectonics (WPI-MANA), National Institute for Materials Science (NIMS), Tsukuba, Ibaraki 304-0044, Japan

Email: tadahiro.komeda.a1@tohoku.ac.jp

Abstract

We constructed a microfluid-assisted solution FET with the channel of atomically thin MoS_2 layers. With the solution FET, we examined the I_d-V_g changes with TCNQ and F4-TCNQ molecules with solvents of IPA and AN. The ΔV_{th}, which is the shift of the threshold voltage of the I_d-V_g curve, shows a significant difference between the TCNQ and F4-TCNQ molecules when measured with IPA solvent. The difference decreases significantly in AN solution. We divide ΔV_{th} into the doping components from the charge transfer and the gating due to the electric field created by the solute. We analyze that most of the significant difference of ΔV_{th} is created by the intra-molecule charge distribution of the F4-TCNQ, which is shielded more efficiently by AN with higher dielectric constant than IP, which is the reason for the reduction of the difference of the ΔV_{th}. This study demonstrates that the solution FET can be employed to solid-solution interface chemistry.

The field effect transistor (FET) using a channel of atomic layer of transition metal dichalcogenide (TMD) attracts attention. TMD-FET is sensitive to channel surface conditions due to the large surface-to-volume ratio. There are great demands for sensor devices, and various sensing mechanisms are proposed.[1-9] FET-based sensor has benefits, including the miniaturization of the device. In addition, the device can be operated in solution environments. The sensitive changes in the electric property of TMD-FET with molecule-electrode interaction can also contribute to a fundamental science of the solution-solid interface, whose experimental analysis is challenging. The interfacial activities of ions are important in physical chemistry, colloidal science, and biophysics.[10] The issues include long-time discussion of an absence of ions in the water/air interface.[11] Pioneered by Wagner [12] and Onsager [13], the ion behavior at the interface has been analyzed considering the electrostatic force for ions at the interface. A key factor for the discussion of ion distribution is the difference in the polarization between the solvent and the bounding medium,[14] where the charge of the ion is directed to the substance with a higher dielectric constant. However, experiments[15] and simulations[16] show that the behavior is ion-specific. Though the recent development of the second harmonic spectroscopy analytical technique provided new experimental insight, the result raises further questions.[17] This suggests a further need for developing the analytical techniques for the solution-solid interface, and the solution-FET experiment can be one of such techniques.

Although the sensor behavior of TMD-FET is studied for a wide variety of molecules, the studies are executed mainly in vacuum and gas environments. A limited number of studies conducted in a solution environment primarily utilize a small volume of a droplet placed on the surface of the channel. The droplet is open to the atmosphere, making less precise results from the solvent's evaporation. Microfluid platform controls solution flow in the sub-mm dimension and provides various advantages for biomaterial sensing.[18-20] TMD-FET equipped with a via hole to the FET channel connected with microfluid can prevent the solution’s contact with the electrodes and evaporation of the solution, making the measurement more precise.[21] A graphene device was demonstrated to provide accurate detection of thrombin.[22]

This report examines the solvation effect of tetracyanoquinodimethane (TCNQ) and 2,3,5,6-Tetrafluoro-7,7,8,8-tetracyanoquinodimethane (F4-TCNQ) molecules for

interaction with MoS_2 using MoS_2-FET with a microfluid tank and optimized solution measurement. Because of their high electron affinity, both molecules are used for molecular electronic devices as p-type dopants.[24-26] In addition, the adsorption of the two molecules is well-studied on metal surfaces.[27-44] We examine the electric property of MoS_2-FET when the MoS_2 channel is in contact with TCNQ and F4-TCNQ solution in isopropyl alcohol (IPA) and acetonitrile (AN). The solution-FET reveals a complex solvation effect between the MoS_2 surface and the solute, originating from the difference in the electrostatic potential distribution between the TCNQ and F4-TCNQ molecules and the different dielectric constant of the IPA and AN. This report is the first study that uses solution-FET for the solvation effect of a solid-liquid interface.

Experimental

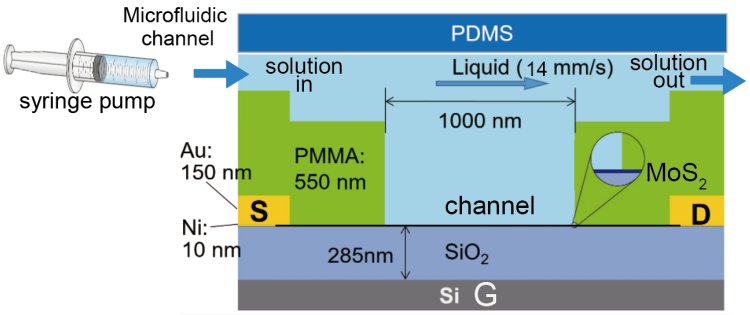

Figure 1 Schematics of the MoS_2-FET device with PMMA via hole and PDMS microfluidic platform.

The device structure is schematically shown in Figure 1. The FET channel is constructed with MoS_2 layers thinner than 4 ML, which is transferred onto the SiO_2 layer (285 nm) by the scotch tape method, whose detail is described in our previous reports. {Trung, 2020 #5086} To restrict the contact of the solution only with the channel, we form the layers of the PMMA A6 with a thickness of 550 nm by the spin coating method. The via hole to the channel of 1 × 1 μm^2 is formed using the electron beam lithography over the MoS_2. A microfluidic tank is constructed with PDMS, which has a size length of 3180 μm and a height of 1100 μm, and a flow area of 50 μm (width) ×40 μm (height). The solution is introduced from a capillary, and a syringe pump controls the velocity of the solution flow. In this experiment, we use the flow of 100 μl/hour (14 mm/s).

We examine the bonding configuration of TCNQ and F4-TCNQ on the MoS_2 surface with the DFT calculation using the VASP code, whose detail is discussed in SI.

Results and discussion

Figure 1(a) shows the changes in the source−drain current (I_d) vs. gate voltage (V_g) characteristic, *i.e.*, the I_d-V_g curve of the microfluid-equipped MoS_2 FET after starting IPA flow, turning a dry MoS_2 channel into a wet condition. With immersing the channel with IPA, the curve shifts towards the positive V_g direction, suggesting that the IPA works as an acceptor-type dopant. The change is slow, and it takes about 10-30 minutes for the curve to stabilize completely. The stabilization time depends on the batch of the device. At this moment, we need to understand the reason for the slow change fully.

After stabilizing the curve, we switch the solution source from the pure IPA to the TCNQ solution, 200 μMol in IPA solvent. IPA is a suitable solvent for TCNQ, where Guillan and coworkers report the solubility of TCNQ in IPA.[45] The I_d-V_g change is illustrated in Figure 2(b), and we observe a clear shift towards the right-hand side, suggesting the acceptor-type behavior by the TCNQ solution. The acceptor behavior of the TCNQ molecule is consistent with the result obtained by the vacuum sublimation of the TCNQ on the MoS_2 channel.[46]

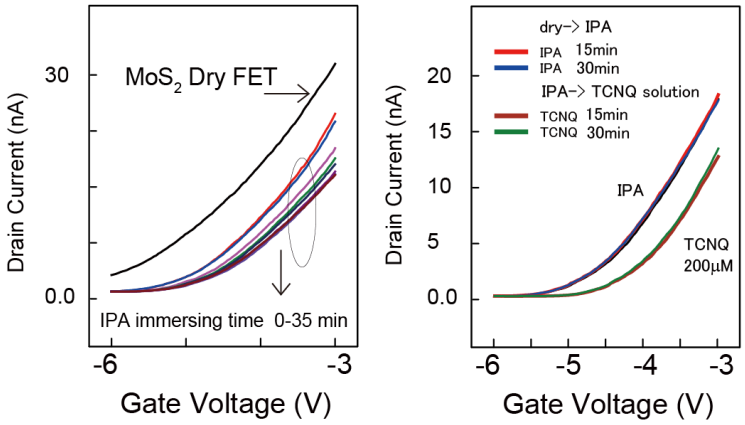

Figure 2. (a) I_d-V_g variation with the time of the immersion of the MoS_2 channel into IPA; the top plot is for the dry channel, and plots in the circle show the changes with time. Time 0 starts the IPA flow in the microfluid onto the dry channel, and the bottoms are obtained after 35 min. (b) Same as (a), but the solution is changed from pure IPA to TCNQ solution in IPA by swapping the syringe after the plot is stabilized in pure IPA.

Here, we compare the behavior of TCNQ and F4-TCNQ molecules, the latter having a slightly higher electron affinity than the former, where four H atoms in the perimeter are replaced with F atoms. Figures 3(a) and (b) illustrate the I_d-V_g plots for different concentrations of the solution of TCNQ, (a), and F4-TCNQ, (b). The acceptor-type doping effect is enhanced with the concentration increase from 50 nM to 100 μM for both molecules. However, we see a clear difference between the two molecules. The

F4-TCNQ molecule has a more enhanced effect as an acceptor than the TCNQ molecule.

The I_d-V_g change is numerically analyzed by estimating the threshold voltage. In a regular FET operation, the drain current rapidly increases at a specific voltage, followed by a linear increase with the gate voltage. The linear part is fitted with a line, and the intersection for the drain current zero is defined as V_{th}.

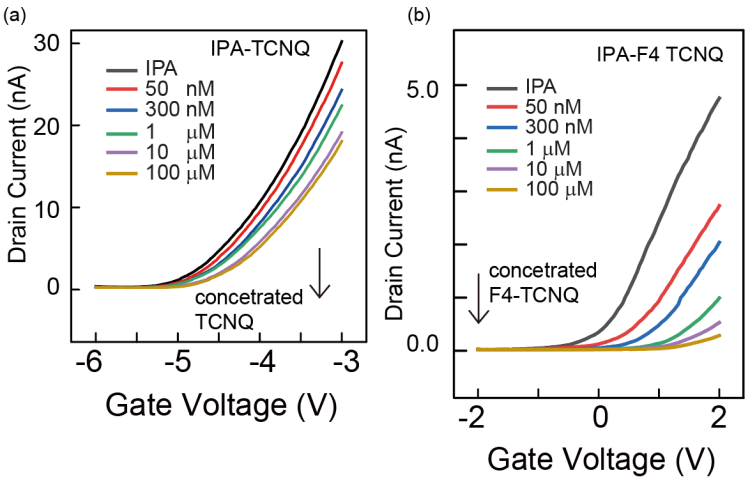

Figure 3. I_d-V_g variation with the different concentrations of TCNQ, (a), and F4-TCNQ solution in IPA. The solution flowed in the microfluid channel during the measurement, and the plots shown in the graphs were measured after stabilization time.

Figure 4(a) plots the change of V_{th} (ΔV_{th}) vs. solution concentrations both for TCNQ and F4-TCNQ in IPA. The uptake curve shows a sharp rise in the nM region and is quickly saturated. The saturated value shows a significant difference, as we checked in Figure 3. The ΔV_{th} change is reversible; if we swap the syringe containing TCNQ/F4-TCNQ solution to pure IPA, the I_d-V_g curve returns to the one for IPA. This is illustrated for the F4-TCNQ case in Figure 4(b), where the syringe was changed at the time marked with arrows in the figure.

Figure 4(c) is a magnified plot of Figure 4(a). The V_{th} shifts towards higher V_g with the concentration. The curve quickly reaches the saturated value for both molecules, whose saturation value is 1.68 eV for F4-TCNQ and 0.40 eV for the TCNQ molecule. For the magnified plot in Figure 4(b), we simulate the ΔV_{th} curve by considering adsorption kinetics by applying a simple Langmuir model. {Langmuir, 1918 #5892}{Azizian, 2018 #5653} In the model, we assume both the TCNQ and F4-TCNQ

molecules form only monolayer and no multilayer. The coverage is defined as N/N_0 using the number of the adsorption sites in the monolayer, N_0, and the adsorbed molecule number, N. We assume that the desorption probability of a single adsorbate is n (1/s). The number of desorbing molecules is $N_0\theta n$. We assume that the molecules adsorb only on the bare part of the substrate. Thus, the number of adsorbed molecules increases proportionally~~proportional~~ to $p_a f_0 N_0(1-\theta)$ where f_0 is the number of the molecules that hit the adsorption site per second, and p_a is the sticking coefficient. In an equilibrium condition, the number of molecules that adsorb on and desorb from the surface should be equal. This condition determines the coverage, which can be expressed as $\theta=\eta/(1+\eta)$ where $\eta= p_a f_0 / n$. Among the three parameters in the right-hand side, only f changes with the concentration. The solid curve expresses the fitting result using this form~~,~~ula reproducing the results for TCNQ and F4-TCNQ with almost equivalent values of p_a and n, except the saturation value. The results indicate that both molecules' adsorption/desorption kinetics follow the same parameters.

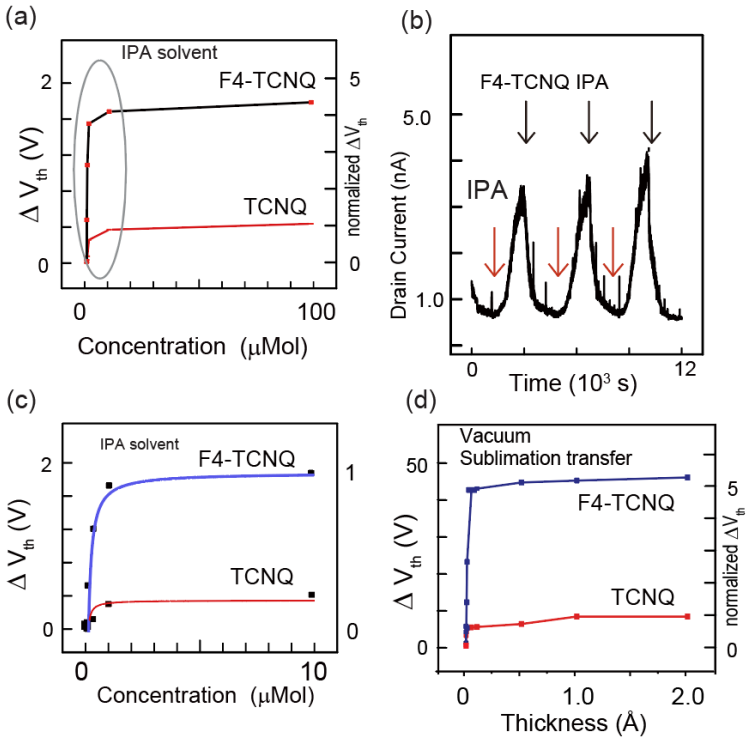

Figure 4 (a) V_{th} variation with the concentration of TCNQ and F4-TCNQ solution (IPA solvent). (b) I_d- variation with switching microfluid solution between pure IPA and F4-TCNQ solution at the red and gray arrows, respectively. (c) The magnified image of (a) with the fitting result is based on a Langmuir model for two molecules (see text). (d)

V_{th} variation with the vacuum sublimation on the MoS_2 channel and measured in the vacuum condition.

The ΔV_{th} value normalized with the saturation value for the TCNQ is illustrated in the right y-axis of Figure 4(a). The saturation V_{th} for F4-TCNQ is 4.2 times higher than that of TCNQ, showing a significant shift. We compare the behavior with the data obtained in the vacuum, and both molecules are transferred with the vacuum sublimation method (Figure 4(d)). In Figure 4(d), the V_{th} saturates quickly for both molecules at the submonolayer region, and the F4-TCNQ molecule shows a 5.2 times higher saturation value than TCNQ. In different words, the difference shrinks in the IPA solution experiment.

The electric property of the TMD-FET changes with the existence of the molecules in the vicinity of the open channel of the TMD atomic layer, which either works as a dopant providing charge transfer between the molecule and the channel or as a gate providing an electrostatic interaction from a dipole moment or ionic state. Both can change the I_d-V_g curve. We can assume that the total shift value of ΔV_{th}(total) is the sum of ΔV_{th}(doping) and ΔV_{th}(gating).

We should examine the origin of the significant difference between the two molecules. The doping effect is expressed as a product of the number of adsorbed molecules and the transferred charge for each molecule. As we examined in the fitting of Figure 4(c), the adsorption kinetics are similar for the two molecules, which rationalizes the assumption of an equal number of adsorbed molecules. The charge transfer for each molecule can be estimated by executing the VASP calculation. Considering the van der Waals interaction, our previous report calculated the charge transfer from the MoS2 substrate to TCNQ and F4-TCNQ molecules in the vacuum condition. {Waizumi, 2022 #5560} The result shows 0.15 and 0.32 e^- per molecule, respectively. [46] We newly execute calculations without the van der Waals force. The molecules are located separated from the MoS_2 surface than in the previous case, and the charge transfers are smaller, 0.020 and 0.044, respectively. Though the absolute values are different, the ratio of the transferred charge is the same, 2.2 times higher for the F4-TCNQ molecule. In a simple model, the ΔV_{th}(doping) should be a linear function of the charge transfer per molecule if we assume the same amount of the adsorbates.

Though the transferred charge ratio explains the larger ΔV_{th}(total) for the F4-TCNQ, it is not large enough. The rest should be originated from the ΔV_{th}(gating).

The charge transfer calculation is done for the vacuum condition. Thus, we must see whether the effect of the solvent modifies the charge transfer difference between the two molecules. To see the impact of solvation by IPA, we employ the VASPsol package,[47, 48] to perform the implicit solvation models (ISM) to represent the TCNQ and F4-TCNQ resolving in IPA solution, in which we assume the dielectric constant of 18 for IPA solvent.[49] The Bader analysis results show that the total charge transfer for TCNQ and F4-TCNQ is 0.020 and 0.038 e^- per molecule. Compared with the vacuum case, the difference is slight, and the value for F4-TCNQ is 16 % decreased, while the one for TCNQ remains the same. The calculated difference is negligible for our discussion.

To see the origin of the gating effect, we calculate the difference in the electrostatic potential mapping (ESP) in the two molecules placed in the vacuum (Figure 5e). A difference in the mapping of the two molecules is evident at the center of the molecule for F4-TCNQ, which is in dark blue, suggesting a high positive potential. Several groups calculate a similar electrostatic potential mapping. {Kurosawa, 2021 #5881;Otero, 2019 #5880} We consider the additional charge segregation in the F4-TCNQ compared to the case of TCNQ as the origin of the ΔV_{th}(gating). As pointed out by Kurosawa and coworkers, the blue-colored region is also prone to nucleophilic attack, at which we should consider interaction with the solvent.

We then examine a solvent with a different dielectric constant from IPA on the variation of the FET properties. We use acetonitrile (AN) solvent for this purpose. A good solubility of the TCNQ in AN was demonstrated by the work of Fink and coworkers, in which a growth mechanism of a charge transfer complex of Ag-TCNQ was demonstrated. The growth mode significantly changed when the solvent was switched to acetone. The mechanism is attributed to a difference in the nucleophilicity of AN and acetone to Ag atom.

We measure the I_d-V_g plot with a microfluid tank using AN. The results are summarized in Figure 5 for two molecules. Figure 5(b)-(e) compares IPA and AN solvents for the concentration of 100 μM, which are in the saturation condition of the I_d-V_g plot. While the difference of ΔV_{th} between the two molecules with IPA solvent is

significant, the difference decreased with the AN solvent. The ΔV_{th} for F4-TCNQ normalized by TCNQ value is 4.8 in IPA but is 1.7 for the AN case.

The dielectric constant of AN is reported as 36,[50], which is more significant than the case of IPA. With a solvent with a higher dielectric constant, the electric field created by the molecule is reduced at the MoS_2 channel. Thus, the ΔV_{th}(gating) component is weakened by this shielding effect, reducing the difference between the two molecules.

As far as we know, a difference in the nucleophilicity of the two solvents for the TCNQ and F4-TCNQ molecules are still being determined; we cannot discuss the effect of different attack by two solvents.

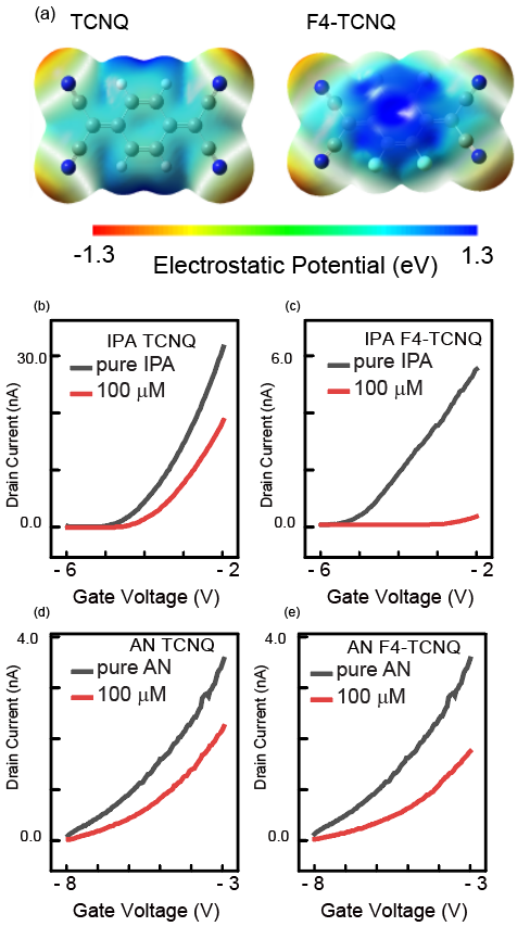

Figure 5 (a) Mapping of the electrostatic potential for TCNQ and F4-TCMQ molecules. The potential is colored following the color bar below, where the blue area is prone to nucleophilic attack. (b)-(e) Effect of the change of the solvents of IPA and acetonitrile

(AN) for TCNQ and F4-TCNQ molecules. The significant difference of the I_d-V_g curves for the TCNQ and F4-TCNQ observed with IPA solvent is much reduced with AN.

As a summary, we constructed a microfluid-assisted solution FET with the channel of atomically thin MoS_2 layers. With the solution FET, we examined the I_d-V_g changes with TCNQ and F4-TCNQ molecules with solvents of IPA and AN. The ΔV_{th}, which is the shift of the threshold voltage of the I_d-V_g curve, shows a significant difference between the TCNQ and F4-TCNQ molecules when measured with IPA solvent. Still, the difference decreases significantly in the AN solution. We divide ΔV_{th} into the doping components from the charge transfer and the gating due to the electric field created by the solute. We analyze that most of the significant difference of ΔV_{th} is created by the intra-molecule charge distribution of the F4-TCNQ, which is shielded more efficiently by AN with a higher dielectric constant than IP, which is the reason for the reduction of the difference of the ΔV_{th}. This study demonstrates that the solution FET can be employed to solid-solution interface chemistry.

1. Rohrbach, F.; Karadeniz, H.; Erdem, A.; Famulok, M.; Mayer, G. *Anal. Biochem.* **2012,** 421, (2), 454-459.
2. Liang, G.; Man, Y.; Jin, X.; Pan, L.; Liu, X. *Anal. Chim. Acta* **2016,** 936, 222-228.
3. Khan, N. I.; Maddaus, A. G.; Song, E. *Biosensors* **2018,** 8, (1).
4. Kokkonen, M.; Jestoi, M.; Rizzo, A. *Food Additives and Contaminants* **2005,** 22, (5), 449-456.
5. Minunni, M.; Tombelli, S.; Gullotto, A.; Luzi, E.; Mascini, M. *Biosensors and Bioelectronics* **2004,** 20, (6), 1149-1156.
6. Liss, M.; Petersen, B.; Wolf, H.; Prohaska, E. *Anal. Chem.* **2002,** 74, (17), 4488-4495.
7. Nakamura, C.; Kobayashi, T.; Miyake, M.; Shirai, M.; Miyake, J. *Molecular Crystals and Liquid Crystals Science and Technology Section A: Molecular Crystals and Liquid Crystals* **2001,** 371, 369-374.
8. McCauley, T. G.; Hamaguchi, N.; Stanton, M. *Anal. Biochem.* **2003,** 319, (2), 244-250.
9. Dittmer, W. U.; Reuter, A.; Simmel, F. C. *Angew. Chem. Int. Ed.* **2004,** 43, (27), 3550-3553.
10. Israelachvili, J. N., *Intermolecular and Surface Forces*. Academic Press: New York, 1992.
11. Jungwirth, P.; Tobias, D. J. *J. Phys. Chem. B* **2002,** 106, (25), 6361-6373.
12. Wagner, C. *Phys. Z* **1924,** 25, 474-477.
13. Onsager, L.; Samaras, N. N. *J. Chem. Phys.* **1934,** 2, (8), 528-536.

14. Son, C. Y.; Wang, Z.-G. *Proc. Natl. Acad. Sci. U.S.A.* **2021,** 118, (19), e2020615118.
15. Jungwirth, P.; Tobias, D. J. *Chem. Rev.* **2006,** 106, (4), 1259-1281.
16. Petersen, P. B.; Saykally, R. J. *Annu. Rev. Phys. Chem.* **2006,** 57, 333-364.
17. McCaffrey, D. L.; Nguyen, S. C.; Cox, S. J.; Weller, H.; Alivisatos, A. P.; Geissler, P. L.; Saykally, R. J. *Proc. Natl. Acad. Sci. U.S.A.* **2017,** 114, (51), 13369-13373.
18. Beebe, D. J.; Mensing, G. A.; Walker, G. M. *Annual Review of Biomedical Engineering* **2002,** 4, 261-286.
19. Sackmann, E. K.; Fulton, A. L.; Beebe, D. J. *Nature* **2014,** 507, (7491), 181-189.
20. Jiang, Y.; Zou, S.; Cao, X. *Analytical Methods* **2016,** 8, (37), 6668-6681.
21. Wang, X.; Hao, Z.; Olsen, T. R.; Zhang, W.; Lin, Q. *Nanoscale* **2019,** 11, (26), 12573-12581.
22. Khan, N. I.; Mousazadehkasin, M.; Ghosh, S.; Tsavalas, J. G.; Song, E. *Analyst* **2020,** 145, (13), 4494-4503.
23. Gao, W.; Kahn, A. *Appl. Phys. Lett.* **2001,** 79, (24), 4040-4042.
24. Rana, O.; Srivastava, R.; Chauhan, G.; Zulfequar, M.; Husain, M.; Srivastava, P. C.; Kamalasanan, M. N. *Physica Status Solidi (A) Applications and Materials Science* **2012,** 209, (12), 2539-2545.
25. Koch, N.; Duhm, S.; Rabe, J. P.; Vollmer, A.; Johnson, R. L. *Phys. Rev. Lett.* **2005,** 95, (23), 237601.
26. Gao, W.; Kahn, A. *J. Appl. Phys.* **2003,** 94, (1), 359-366.
27. Blowey, P. J.; Velari, S.; Rochford, L. A.; Duncan, D. A.; Warr, D. A.; Lee, T. L.; De Vita, A.; Costantini, G.; Woodruff, D. P. *Nanoscale* **2018,** 10, (31), 14984-14992.
28. Yamane, H.; Kosugi, N. *J. Phys. Chem. Lett.* **2017,** 8, (21), 5366-5371.
29. Gerbert, D.; Maaß, F.; Tegeder, P. *J. Phys. Chem. C* **2017,** 121, (29), 15696-15701.
30. Borghetti, P.; Sarasola, A.; Merino-DÍez, N.; Vasseur, G.; Floreano, L.; Lobo-Checa, J.; Arnau, A.; De Oteyza, D. G.; Ortega, J. E. *J. Phys. Chem. C* **2017,** 121, (51), 28412-28419.
31. Gerbert, D.; Tegeder, P. *J. Phys. Chem. Lett.* **2017,** 8, (19), 4685-4690.
32. Stradi, D.; Borca, B.; Barja, S.; Garnica, M.; Díaz, C.; Rodríguez-García, J. M.; Alcamí, M.; Vázquez De Parga, A. L.; Miranda, R.; Martín, F. *RSC Advances* **2016,** 6, (18), 15071-15079.
33. Feyer, V.; Graus, M.; Nigge, P.; Zamborlini, G.; Acres, R. G.; Schöll, A.; Reinert, F.; Schneider, C. M. *J. Electron Spectrosc. Relat. Phenom.* **2015,** 204, 125-131.
34. Sun, Z.; Zhan, Y.; Shi, S.; Fahlman, M. *Organic Electronics* **2014,** 15, (9), 1951-1957.
35. Park, C.; Rojas, G. A.; Jeon, S.; Kelly, S. J.; Smith, S. C.; Sumpter, B. G.; Yoon, M.; Maksymovych, P. *Phys. Rev. B* **2014,** 90, (12), 125432.
36. Burema, S. R.; Bocquet, M. L. *Phys. Chem. Chem. Phys.* **2013,** 15, (38), 16111-16119.
37. Barja, S.; Stradi, D.; Borca, B.; Garnica, M.; Díaz, C.; Rodriguez-García, J. M.; Alcamí, M.; Vázquez De Parga, A. L.; Martín, F.; Miranda, R. *J. Phys. Condens. Matter* **2013,** 25, (48), 484007.

38. Faraggi, M. N.; Jiang, N.; Gonzalez-Lakunza, N.; Langner, A.; Stepanow, S.; Kern, K.; Arnau, A. *J. Phys. Chem. C* **2012,** 116, (46), 24558-24565.
39. Wäckerlin, C.; Iacovita, C.; Chylarecka, D.; Fesser, P.; Jung, T. A.; Ballav, N. *Chem. Commun.* **2011,** 47, (32), 9146-9148.
40. Katayama, T.; Mukai, K.; Yoshimoto, S.; Yoshinobu, J. *Phys. Rev. B* **2011,** 83, (15), 153403.
41. Katayama, T.; Mukai, K.; Yoshimoto, S.; Yoshinobu, J. *J. Phys. Chem. Lett.* **2010,** 1, (19), 2917-2921.
42. Rangger, G. M.; Hofmann, O. T.; Romaner, L.; Heimel, G.; Bröker, B.; Blum, R. P.; Johnson, R. L.; Koch, N.; Zojer, E. *Phys. Rev. B* **2009,** 79, (16), 165306.
43. Romaner, L.; Heimel, G.; Brédas, J. L.; Gerlach, A.; Schreiber, F.; Johnson, R. L.; Zegenhagen, J.; Duhm, S.; Koch, N.; Zojer, E. *Phys. Rev. Lett.* **2007,** 99, (25), 256801.
44. Erley, W.; Ibach, H. *Surf. Sci.* **1986,** 178, (1-3), 565-577.
45. Guillain, F.; Endres, J.; Bourgeois, L.; Kahn, A.; Vignau, L.; Wantz, G. *ACS Applied Materials and Interfaces* **2016,** 8, (14), 9262-9267.
46. Waizumi, H.; Shamim Al Mamun, M.; Takaoka, T.; Iftekharul Alam, M.; Tanaka, Y.; Ando, A.; Wang, Z.; Arafune, R.; Komeda, T. *Appl. Surf. Sci.* **2022,** 571.
47. Mathew, K.; Sundararaman, R.; Letchworth-Weaver, K.; Arias, T. A.; Hennig, R. G. *J. Chem. Phys.* **2014,** 140, (8), 084106.
48. Mathew, K.; Kolluru, V. S. C.; Mula, S.; Steinmann, S. N.; Hennig, R. G. *J. Chem. Phys.* **2019,** 151, (23), 234101.
49. Park, J.-G.; Lee, S.-H.; Ryu, J.-S.; Hong, Y.-K.; Kim, T.-G.; Busnaina, A. A. *J. Electrochem. Soc.* **2006,** 153, (9), G811.
50. Miller, C. G.; Maass, O. *Can. J. Chem.* **1960,** 38, (9), 1606-1616.